Inorg. Chem. **2007**, *46*, 9646–9654

Thermal- and Pressure-Induced Cooperative Spin Transition in the 2D and 3D Coordination Polymers $\{Fe(5\text{-Br-pmd})_z[M(CN)_x]_y\}$ (M = Ag^I, Au^I, Ni^{II}, Pd^{II}, Pt^{II})

Gloria Agustí,[†] Ana Belén Gaspar,[†] M. Carmen Muñoz,[‡] and José Antonio Real*[,†]

Institut de Ciència Molecular/Departament de Química Inorgànica, Universitat de València, Edifici de Instituts de Paterna, Apartat de Correus 22085, 46071 València, Spain, and Departament de Física Aplicada, Universitat Politécnica de València, Camí de Vera s/n, 46022 València, Spain

Received May 22, 2007

A new family of cyanide-based spin-crossover polymers with the general formula $\{Fe(5\text{-Br-pmd})_z[M(CN)_x]_y\}$ [M = Ag^I (**1**), Au^I (**2**), Ni^{II} (**3**), Pd^{II} (**4**), Pt^{II} (**5**); 5-Br-pmd = 5-bromopyrimidine; $z = 1$ or 2, $x = 2$ or 4, and $y = 2$ or 1] have been synthesized and characterized using single-crystal X-ray diffraction (XRD), X-ray powder diffraction (XRPD), magnetic susceptibility measurements, and differential scanning calorimetry (DSC). At 293 K, compound **1** presents the monoclinic space group *C*2/*c*, whereas at 120 K, it changes to the monoclinic space group $P2_1/c$. At 293 K, the crystal structure of **1** displays an uninodal three-dimensional network whose nodes, constituted of Fe^{II}, lie at the inversion center of an elongated octahedron. The equatorial bond lengths are defined by the N atoms of four $[Ag^I(CN)_2]^-$ groups belonging to two crystallographically nonequivalent Ag^I atoms, Ag(1) and Ag(2). They are shorter than those of the axial positions occupied by the N atoms of the 5-Br-pmd ligands. The Fe–N average bond length of 2.1657(7) Å is consistent with a high-spin (HS) state for the Fe^{II} ions. At 120 K, the crystal structure changes refer mainly to the Fe^{II} environment. There are two crystallographically independent Fe^{II} ions at this temperature, Fe(1) and Fe(2), which adopt the HS and low-spin (LS) states, respectively. The average Fe–N bond length for Fe(1) [2.174(5) Å] and Fe(2) [1.955(5) Å] agrees well with the reported magnetic data at this temperature. The spin transition of the Fe^{II} ions labeled as Fe(1) is found to be centered at $T_c^{\downarrow} = 149$ K and $T_c^{\uparrow} = 167$ K and accompanied by a drastic change of color from orange (HS) to red (LS). Magnetic susceptibility measurements under applied hydrostatic pressure performed on **1** have shown a linear displacement of the transition to higher temperatures while the hysteresis width remains unaltered in the interval of pressures of 10^5 Pa to 0.34 GPa. A further increase of the pressure induces the spin transition in the Fe(2) ions, which is completely accomplished at 1.12 GPa ($T_{1/2} = 162$ K). Compounds **1** and **2** are isostructural, but **2** does not exhibit spin-transition properties; the Fe^{II} centers remain in the HS state in the temperature range investigated, 5–300 K. Compounds **3**–**5** are not similar or isostructural with **1**. A two-dimensional structure for **3**–**5** has been proposed on the basis of analytical data and the XRPD patterns. Compounds **3**–**5** undergo first-order spin transition where the critical temperatures for the cooling ($T_c^{\downarrow}$) and warming ($T_c^{\uparrow}$) modes are 170 and 180 K (**3**), 204 and 214 K (**4**), and 197 and 223 K (**5**), respectively. It is worth mentioning the color change from yellow to orange observed in **3**–**5** upon spin transition. The thermodynamic parameters associated with the spin transition estimated from DSC measurements are $\Delta H =$ 6 kJ mol^{-1} (**1**), 11 kJ mol^{-1} (**3**), 16 kJ mol^{-1} (**4**), and 16 kJ mol^{-1} (**5**) and $\Delta S = 38$ J K^{-1} mol^{-1} (**1**), 62 J K^{-1} mol^{-1} (**3**), 76 J K^{-1} mol^{-1} (**4**), and 81 J K^{-1} mol^{-1} (**5**).

Introduction

Functional materials with switch properties and memory transduction have considerable interest in view of their potential technological applications.[1] Despite the fact that an important number of coordination polymers with specific topologies have recently been reported,[2] incorporation of

* To whom correspondence should be addressed. E-mail: jose.a.real@uv.es.
[†] Universitat de València.
[‡] Universitat Politécnica de València.

(1) (a) Hollingsworth, M. D. *Science* **2002**, *295*, 2410. (b) Janiak, C. *J. Chem. Soc., Dalton Trans.* **2003**, 2781.
(2) (a) Batten, S. R.; Robson, R. *Angew. Chem., Int. Ed.* **1998**, *37*, 1460. (b) Robson, R. *J. Chem. Soc., Dalton Trans.* **2000**, 3735. (c) Zaworotko, M. J. *Chem. Commun.* **2001**, 1. (d) Yaghi, O. M.; Li, H.; Davis, C.; Richardson, D.; Groy, T. L. *Acc. Chem. Res.* **1998**, *31*, 474. (e) Eddaoudi, M.; Moler, D. B.; Li, H.; Chen, B.; Reineke, T. M.; O'Keeffe, M.; Yaghi, O. M. *Acc. Chem. Res.* **2001**, *34*, 319.

10.1021/ic700993s CCC: $37.00 © 2007 American Chemical Society
Published on Web 10/10/2007

mechanically, electronically, or optically active building blocks as essential structural components in the construction of such functional materials has been scarcely explored.[3] In this regard, the use of spin-crossover (SCO) building blocks for the construction of functional coordination polymers has been shown as a suitable strategy because they change reversibly their magnetic, structural, dielectric, and optical properties in response to stimuli such as a variation of temperature or pressure and light irradiation.[4−7]

The necessity of improving communication between the active SCO centers has prompted the search for new synthetic strategies to obtain not only more rigid networks but also more chemically and structurally versatile systems. For instance, the possibility of inducing polymerization through suitable coordinated anions, i.e., cyanide ligands, has been considered only recently.

Cyanide-bridged homo- and heterometallic coordination polymers have been shown to exhibit a remarkable diversity of structural types with interesting magnetic, electrochemical, magneto-optical, thermomechanical, and zeolitic properties.[8] In particular, Hofmann-like clathrate compounds[9] containing Fe^{II} ions have led to the development of a number of two-dimensional (2D) $\{Fe(pyridine)_2[M^{II}(CN)_4]\}$[10,11a] and three-dimensional (3D) $\{Fe(pyrazine)[M^{II}(CN)_4]\}\cdot nH_2O$[11] frameworks where M^{II} is Ni, Pd, or Pt. The pyrazine derivatives undergo abrupt thermal-, pressure-, and light-induced SCO[11d] behavior with thermal hysteresis close to room temperature,[11a−c] which confers them bistability, an essential property for the construction of advanced materials with potential applications. The formal replacement of the $[M^{II}(CN)_4]^{2-}$ anions by $[M^I(CN)_2]^-$ groups (M^I = Cu, Ag, Au), with *trans*-bis(pyridyl)ethylene, 4,4′-bipyridine, 3-cyanopyridine, or pyrimidine (pmd) as ligands, has afforded new 2D and 3D SCO polymers.[12−20] Such compounds not only display interesting pressure- and light-induced properties,[14−19] but they can also combine their cooperative spin-transition properties (magnetic, chromatic, and structural) with different chemical properties such as crystalline-state ligand-substitution reactions with remarkable structural changes[13b] or metallophilicity.[14] Most of the above referred $\{Fe^{II}L[M^I(CN)_2]\}$ systems are based on the $[Ag(CN)_2]^-$ or $[Au(CN)_2]^-$ building blocks. In fact, only two SCO coordination polymers based on $[Cu(CN)_2]^-$ have been investigated so far.[18,20]

As a continuation of this research line, we present here the synthesis and characterization of a new family of cyanide-based SCO polymers with the general formula $\{Fe(5\text{-Br-pmd})_z[M(CN)_x]_y\}$ [M = Ag^I (**1**), Au^I (**2**), Ni^{II} (**3**), Pd^{II} (**4**), Pt^{II} (**5**); 5-Br-pmd = 5-bromopyrimidine; $z = 1$ or 2, $x = 2$ or 4, and $y = 2$ or 1].

Results

Crystal Structure of 1 at 293 and 120 K. The crystal structure determinations were performed at 293 and 120 K for polymer **1**. At 293 K, **1** displays the monoclinic space group *C*2/*c*, whereas at 120 K, it changes to the monoclinic space group $P2_1/c$. A selection of crystallographic data and bond distances and angles is given in Tables 1 and 2. The structure of **1** can be described as a 3D network, where the Fe^{II} ions are the nodes (4 + 2 connection). Topologically,[21] it is described as $\{4^4.6^{10}.8\}$ (Schläfli symbol) or $[4.4.4.4.6_2.6_5.6_5.6_5.6_5.6_6.6_7.6_7.6_{11}.6_{11}.*]$ (long topological O'Keeffe vertex symbol).[22]

Figure 1 displays an ORTEP view around the Fe^{II} center at 293 K with the corresponding atom numbering scheme. The Fe atom lies at the inversion center of an elongated octahedron. The equatorial bond lengths are defined by the N atoms of four $[Ag^I(CN)_2]^-$ groups belonging to two crystallographically nonequivalent Ag^I atoms, Ag(1) and Ag(2). They are shorter than those of the axial positions occupied by the N atoms of the 5-Br-pmd ligands [$Fe-N(1)_{eq}$ = 2.118(6), $Fe-N(2)_{eq}$ = 2.108(8) Å, and $Fe-N(3)_{ax}$ = 2.271(6) Å]. The Ag−C bond distances are Ag(1)−C(1) =

(3) (a) Kitagawa, S.; Kitaura, R.; Noro, S. *Angew. Chem., Int. Ed.* **2004**, *43*, 2334. (b) Beauvais, L. G.; Long, J. R. *J. Am. Chem. Soc.* **2002**, *124*, 12098. (c) Langley, P. J.; Hulliguer, J. *Chem. Soc. Rev.* **1999**, *28*, 279.

(4) Gütlich, P.; Goodwin, H. A. Spin Crossover in Transition Metal Compounds. *Top. Curr. Chem.* **2004**, *233*, *234*, *235*.

(5) (a) Real, J. A.; Gaspar, A. B.; Muñoz, M. C. *Dalton Trans.* **2005**, 2062. (b) Gaspar, A. B.; Ksenofontov, V.; Seredyuk, M.; Gütlich, P. *Coord. Chem. Rev.* **2005**, *249*, 2661.

(6) Real, J. A.; Gaspar, A. B.; Niel, V.; Muñoz, M. C. *Coord. Chem. Rev.* **2003**, *236*, 121.

(7) Gütlich, P.; Hauser, A.; Spiering, H. *Angew. Chem., Int. Ed. Engl.* **1994**, *33*, 2024.

(8) (a) Dunbar, K. R.; Heintz, R. A. *Prog. Inorg. Chem.* **1997**, *45*, 283. (b) Sato, O. *J. Photochem. Photobiol. C* **2004**, *5*, 203. (c) Margadonna, S.; Prassides, K.; Fitch, A. N. *J. Am. Chem. Soc.* **2004**, *126*, 15390. (d) Goodwin, A. L.; Chapman, K. W.; Kepert, C. J. *J. Am. Chem. Soc.* **2005**, *127*, 17980.

(9) Iwamoto, T. In *Inclusion Compounds*; Atwood, J. L., Davies, J. E. D., MacNicol, D. D., Eds.; Oxford University Press: London, U.K., 1991; Vol. 5, p 177.

(10) Kitazawa, T.; Gomi, Y.; Takahashi, M.; Takeda, M.; Enemoto, A.; Miyazaki, T.; Enoki, T. *J. Mater. Chem.* **1996**, *6*, 119.

(11) (a) Niel, V.; Martinez-Agudo, J. M.; Muñoz, M. C.; Gaspar, A. B.; Real, J. A. *Inorg. Chem.* **2001**, *40*, 3838. (b) Molnar, G.; Niel, V.; Gaspar, A. B.; Real, J. A.; Zwick, A.; Bousseksou, A.; McGarvey, J. J. *J. Phys. Chem. B* **2002**, *106*, 9701. (c) Molnar, G.; Niel, V.; Real, J. A.; Dubrovinsky, L.; Bousseksou, A.; McGarvey, J. J. *J. Phys. Chem. B* **2003**, *107*, 3149. (d) Bonhommeau, S.; Molnár, G.; Galet, A.; Zwick, A.; Real, J. A.; McGarvey, J. J.; Bousseksou, A. *Angew. Chem., Int. Ed.* **2005**, *44*, 2.

(12) Niel, V.; Muñoz, M. C.; Gaspar, A. B.; Galet, A.; Levchenko, G.; Real, J. A. *Chem.—Eur. J.* **2002**, *11*, 2446.

(13) (a) Niel, V.; Galet, A.; Gaspar, A. B.; Muñoz, M. C.; Real, J. A. *Chem. Commun.* **2003**, 1248. (b) Niel, V.; Thompson, A. L.; Muñoz, M. C.; Galet, A.; Goeta, A. E.; Real, J. A. *Angew. Chem. Int. Ed.* **2003**, *42*, 3759.

(14) Niel, V.; Thompsom, A. L.; Galet, A.; Enachescu, C.; Muñoz, M. C.; Hauser, A.; Goeta, A. E.; Real, J. A. *Chem.—Eur. J.* **2005**, *11*, 2047.

(15) Galet, A.; Muñoz, M. C.; Gaspar, A. B.; Real, J. A. *Inorg. Chem.* **2005**, *44*, 8749.

(16) Galet, A.; Niel, V.; Muñoz, M. C.; Real, J. A. *J. Am. Chem. Soc.* **2003**, *125*, 14224.

(17) (a) Galet, A.; Muñoz, M. C.; Martínez, V.; Real, J. A. *Chem. Commun.* **2004**, 2268. (b) Galet, A.; Muñoz, M. C.; Real, J. A. *Chem. Commun.* **2006**, 4321.

(18) Niel, V.; Galet, A.; Gaspar, A. B.; Muñoz, M. C.; Real, J. A. *Chem. Commun.* **2003**, 1248.

(19) Galet, A.; Gaspar, A. B.; Muñoz, M. C.; Bukin, G. V.; Levchenko, G.; Real, J. A. *Adv. Mater.* **2005**, *17*, 2949.

(20) Galet, A.; Muñoz, M. C.; Real, J. A. *Inorg. Chem.* **2006**, *45*, 4583.

(21) (a) Carlucci, L.; Ciani, G.; Proserpio, D. M. *Coord. Chem. Rev.* **2003**, *246*, 247. (b) Blatov, V. A.; Shevchenko, A. P.; Serezhkin, V. N. *J. Appl. Crystallogr.* **2000**, *33*, 1193. (c) Blatov, V. A.; Carlucci, L.; Ciani, G.; Proserpio, D. M. *CrystEngComm* **2004**, *65*, 377. (d) Delgado-Friedrichs, O.; O'Keeffe, M. *Acta Crystallogr., Sect. A* **2003**, *A59*, 351.

(22) Dolomanov, O. V.; Blake, A. J.; Champness, N. R.; Schröder, M. *J. Appl. Crystallogr.* **2003**, *36*, 1283.

Table 1. Crystal Data for **1** at 293 and 120 K[a]

	293 K	120 K
formula	$C_8H_3N_6FeBrAg_2$	$C_8H_3N_6FeBrAg_2$
M_r	534.66	534.66
cryst syst	monoclinic	monoclinic
space group	*C*2/*c*	$P2_1/c$
a (Å)	14.5280(6)	11.9230(3)
b (Å)	14.8730(8)	14.6690(7)
c (Å)	7.9490(5)	8.0680(5)
β (deg)	121.612(2)	92.211(3)
V (Å^3)	1462.72(14)	1410.03(12)
Z	4	4
D_c (mg cm^{-3})	2.428	2.519
F(000)	992	992
μ(Mo Kα) (mm^{-1})	6.350	6.588
cryst size (mm)	0.03 × 0.06 × 0.09	0.03 × 0.06 × 0.09
T (K)	293(2)	120(2)
no. of total reflns	1528	3220
no. of reflns [$I > 2\sigma(I)$]	1248	2506
R1 [$I > 2\sigma(I)$]	0.0593	0.0410
wR2	0.1635	0.0951
S	1.034	1.010

[a] $R1 = \sum||F_o| - |F_c||/\sum|F_o|$; $wR2 = [\sum[w(F_o^2 - F_c^2)^2]/\sum[w(F_o^2)^2]]^{1/2}$, $w = 1/[\sigma^2(F_o^2) + (mP)^2 + nP]$, where $P = (F_o^2 + 2F_c^2)/3$; $m = 0.1056$ [**1** (293 K)], 0.0471 [**1** (120 K)]; $n = 10.7989$ [**1** (293 K)], 7.1652 [**1** (120 K)].

Table 2. Selected Bond Lengths [Å] and Angles [deg] for **1** at 293 and 150 K

293 K		150 K	
Fe−N(1)	2.118(6)	Fe(1)−N(1)	2.120(5)
Fe−N(2)	2.108(8)	Fe(1)−N(2)	2.116(5)
Fe−N(3)	2.271(6)	Fe(1)−N(3)	2.285(5)
		Fe(2)−N(4)	1.999(4)
		Fe(2)−N(5)	1.932(5)
		Fe(2)−N(6)	1.934(5)
average Fe−N distance	2.1657(7)	Fe(1)	2.174(5)
		Fe(2)	1.955(5)
N(1)-Fe−N(2)	87.8(3)	N(1)−Fe(1)−N(2)	91.6 (2)
N(1)-Fe−N(3)	90.4(2)	N(1)−Fe(1)−N(3)	91.6 (2)
N(2)-Fe−N(3)	88.2(3)	N(2)−Fe(1)−N(3)	93.0(2)
		N(4)−Fe(2)−N(5)	88.6 (2)
		N(4)−Fe(2)−N(6)	90.1(2)
		N(5)−Fe(2)−N(6)	89.1(2)

2.055(7) Å and Ag(2)−C(2) = 2.048(10) Å, whereas the corresponding C−N distances are C(1)−N(1) = 1.140(9) Å and C(2)−N(2) = 1.149(12) Å. The Fe−N average bond length of 2.1657(7) Å is consistent with a high-spin (HS) state for the Fe^{II} ions and matches with the reported magnetic data at this temperature (vide infra). Given its intricate structure, we have deconstructed the network in several significant fragments. The 5-Br-pmd molecule acts as a bis-monodentate ligand linking two consecutive Fe^{II} centers, as depicted in Figure 2a. The coordination of the Fe^{II} node to the nonlinear $[Ag(2)(CN)_2]^-$ groups [C(2)−Ag(2)−C(2^i) = 168.8(5)° ($i = 1 - x, y, -z - {}^1/_2$)] and to the 5-Br-pmd ligands leads to the formation of $\{Fe(Br\text{-}pmd)(Ag(2)(CN)_2)\}_\infty$ sheets, lying in the *xz* plane (Figure 2b), which are pillared along the *y* direction by the $[Ag(1)(CN)_2]^-$ groups [C(1)−Ag(1)−C(1^i) = 180.0(4)° ($i = 1 - x, 1 - y, 1 - z$)]. These sheets are made up of edge-sharing rhombuses $\{Fe_2(Br\text{-}pmd)\text{-}(Ag(2)(CN)_2)\}_2$, where the distances Fe−Br-pmd−Fe^i and Fe−Ag(2)−Fe^{ii} are 6.1884(3) and 9.9412(4) Å, respectively ($i = -x, y, -z - {}^1/_2$, ii = $-x, y, -z + {}^1/_2$). The complementary angles of this pseudorhombus are 125(1)° and 55(1)°. Figure 2c emphasizes the undulated nature of these planes imposed by the nonlinear $[Ag(2)(CN)_2]^-$ groups and the particular zigzag disposition of the 5-Br-pmd ligands with respect to the Fe nodes. The $[Ag(1)(CN)_2]^-$ groups link the sheets along the *y* direction, generating the 3D structure illustrated in Figure 3. The $[Ag(1)(CN)_2]^-$ groups are disposed in such a way that they form an angle of 45° with the edge *y* of the crystal.

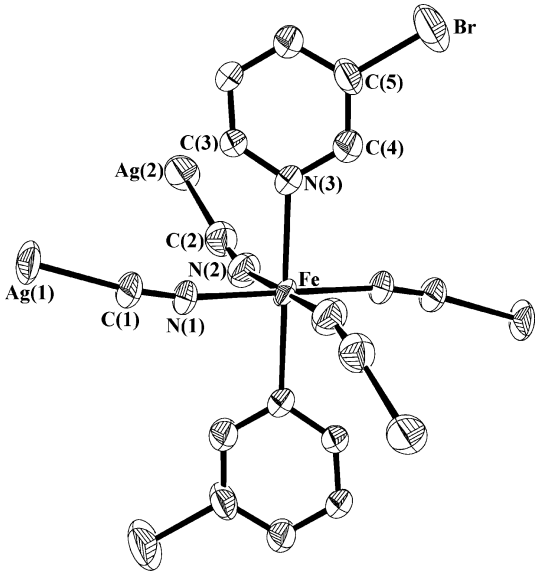

Figure 1. Perspective view of the representative fragment of compound **1** around the Fe^{II} center with the corresponding atom numbering scheme (293 K). Displacement ellipsoids are shown at 50% probability levels.

At 120 K, compound **1** adopts the monoclinic space group $P2_1/c$, but the crystal structure changes mainly involve the Fe^{II} environment. Figure 4 displays an ORTEP view around the Fe^{II} centers at 150 K with the corresponding atom numbering scheme. There are two crystallographically independent Fe^{II} ions at this temperature, Fe(1) and Fe(2). The average Fe−N bond length for Fe(1) [2.174(5) Å] and Fe(2) [1.955(5) Å] agrees well with the Fe−N bond distances typically found for an Fe^{II} ion in the HS and low-spin (LS) states, respectively. This singular fact perfectly correlates with the reported magnetic data at this temperature. Figure 5 illustrates the $\{Fe(1)Fe(2)(Br\text{-}pmd)(Ag(2)(CN)_2)\}_\infty$ sheet in the *xz* plane. Because of the LS configuration adopted by the Fe(2) ion, the distances Fe(1)−Br-pmd−Fe(2) and Fe-(1)−Ag(2)−Fe(2) are shorter at this temperature in comparison with those at 293 K [5.962(1) and 9.845(1) Å, respectively]. Also, there are slight modifications of the NC−Ag−CN angles and bond distances. The Ag−C bond distances are Ag(1)−C(1) = 2.051(5) Å [Ag(1)−C(8) = 2.045(5) Å] and Ag(2)−C(2) = 2.055(6) Å [Ag(2)−C(7) = 2.061(6) Å], whereas the corresponding C−N distances are C(1)−N(1) = 1.158(7) Å, C(8)−N(6) = 1.162(7) Å, C(2)−N(2) = 1.142(8) Å, and C(7)−N(5) = 1.147(7) Å. Both $[Ag(1)(CN)_2]^-$ and $[Ag(2)(CN)_2]^-$ groups are more bent at this temperature, being C(1)−Ag(1)−C(8^i) = 178.5(2)° ($i = x, -y - {}^1/_2, z + {}^1/_2$) and C(2)−Ag(2)−C(7^i) = 167.4(2)° ($i = 1 - x, -y, 1 - z$). These structural parameters are

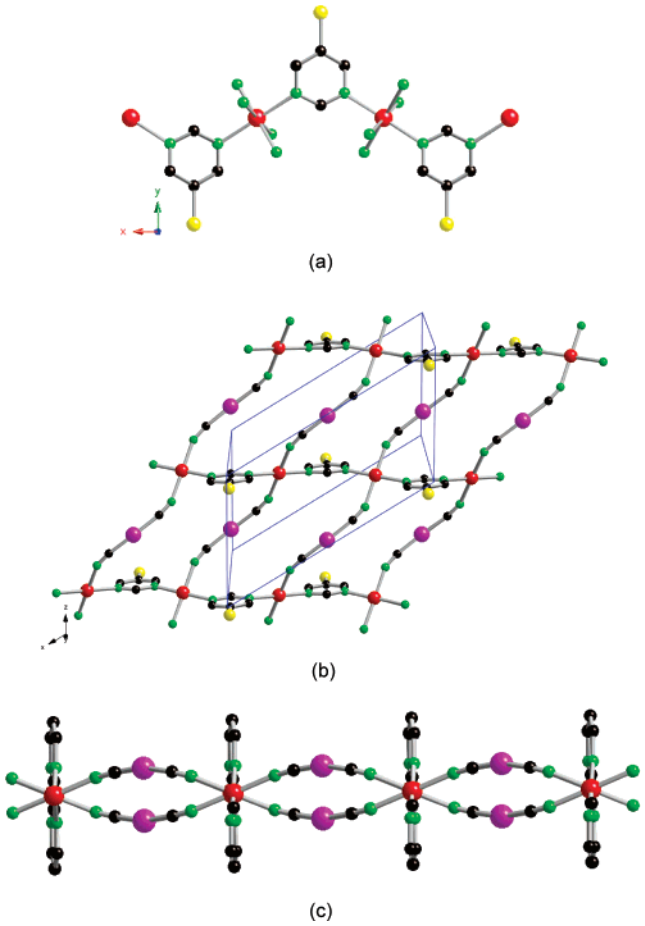

Figure 2. Illustration of the structure of compound **1** at 293 K: (a) view of the [Fe−pmd−Fe]$_n$ fragment in the *x* direction; (b) view of the 2D fragment of {[Fe(pmd)(Ag(2)(CN)$_2$)}$_n$ in the *xz* plane where the nodes are the Fe^{II} centers; (c) perspective view in the *y* direction of the undulated 2D fragments of {[Fe(pmd)(Ag(2)(CN)$_2$)}$_n$. Atom code: Fe, red; Ag(2), magenta; C, black; N, green; Br, yellow. The [Ag(1)(CN)$_2$]$^-$ groups are depicted as gray rods.

similar to those observed previously for other iron(II) dicyanoargentate systems.[12−19]

X-ray Powder Diffraction (XRPD). Powder XRD patterns for **1**−**5** were recorded at 293 K (Figures SM1 and SM2, Supporting Information). Compounds **1** and **2** have very similar profiles, where the representative peaks are as follows: 2θ = 9.30°, 14.30°, 18.70°, 18.95°, 19.44°, and 22.50°. From these XRPD profiles, one can conclude that compounds **1** and **2** are isostructural. Compounds **3**−**5** have quite similar patterns, but they do not match at all that of **1**, denoting that they are not isostructural. In all of them were found common intense peaks located at about the same values in the ranges of 11−12°, 18−19°, and 21−24° (2θ = 11.80°, 13.15°, 18.50°, 21.91°, and 24.15°), which point out that the same structure seems to be the case in all of these compounds. Taking into account the analytical data of compounds **3**−**5** and the XRPD patterns, it is reasonable to propose a 2D structure similar to that reported for [Fe(py)$_2$(M(CN)$_4$)] (M = Ni^{II},[10] Pd^{II},[11] Pt^{II} [11]). In fact, the XRPD patterns of the latter compounds at 293 K show peaks at values of 2θ in the ranges 11−12°, 18−19°, and 21−24°, which correspond to the Fe−Fe, Fe−M^{II}, and Pt−C distances, respectively.

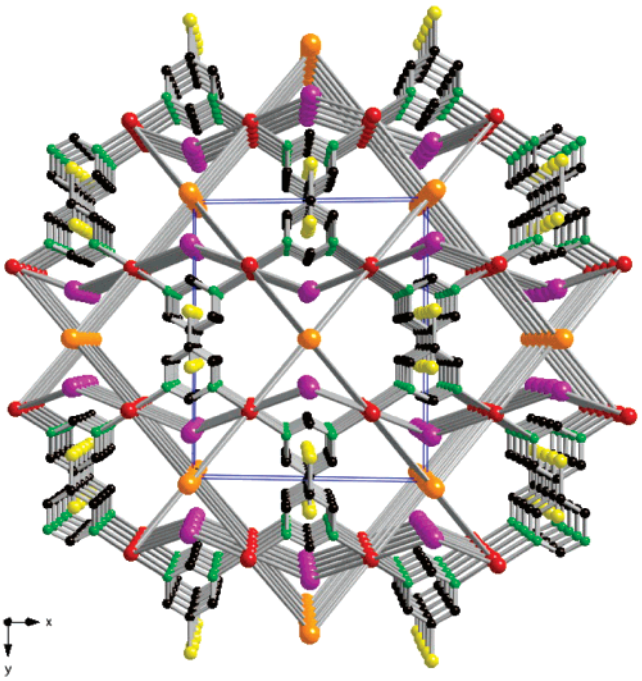

Figure 3. Perspective view of the 3D structure of **1**. The linear [Ag(1)(CN)$_2$]$^-$ groups link the 2D fragments of {[Fe(pmd)(Ag(2)(CN)$_2$)}$_n$ pillared in the *y* direction, leading to the 3D structure where the nodes are the six-connected Fe^{II} ions. Atom code: Fe, red; Ag(1), orange; Ag(2), magenta; C, black; N, green; Br, yellow. The [Ag(1)(CN)$_2$]$^-$ groups are depicted as gray rods.

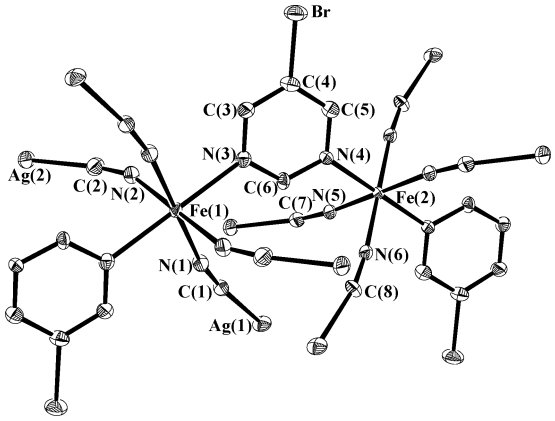

Figure 4. Perspective view of the representative fragment of compound **1** around the Fe(1) and Fe(2) centers with the corresponding atom numbering scheme (120 K). Displacement ellipsoids are shown at 50% probability levels.

Magnetic Properties. The magnetic data expressed in the form of $\chi_M T$ vs T, with χ_M being the molar magnetic susceptibility and T the temperature, at different pressures are shown in Figure 6 for compound **1**. The temperature dependence of the magnetic susceptibility was recorded on a microcrystalline sample over the 5−300 K range in a field of 1 T at a rate of 1 K min^{-1}. At atmospheric pressure (10^5 Pa) and 300 K, the $\chi_M T$ value is 3.55 cm^3 K mol^{-1}. This value remains constant down to 160 K, at which an abrupt decrease of $\chi_M T$ takes place within few Kelvin because of the spin transition of the Fe^{II} ions labeled as Fe(1) ($\chi_M T$ = 1.82 cm^3 K mol^{-1} at 145 K). A second decrease of $\chi_M T$ is observed at around 55 K, which corresponds to the zero-field splitting of the metallic centers remaining in the HS

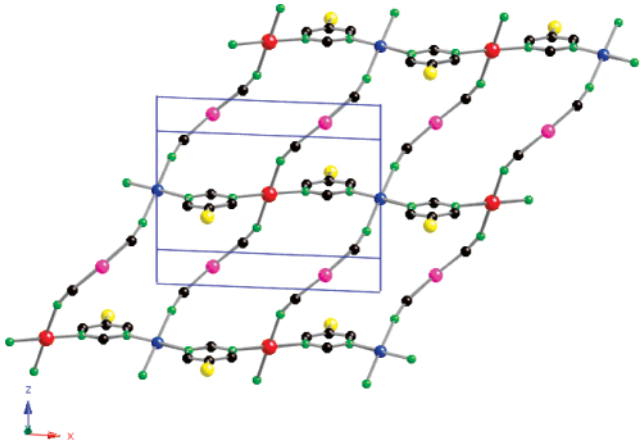

Figure 5. View of the 2D fragments of $\{[Fe(pmd)(Ag(CN)_2)\}_n$ in the *xz* plane where the nodes are the Fe^{II} centers. Atom code: Fe(HS state), red; Fe(LS state), blue; Ag(2), magenta; C, black; N, green; Br, yellow.

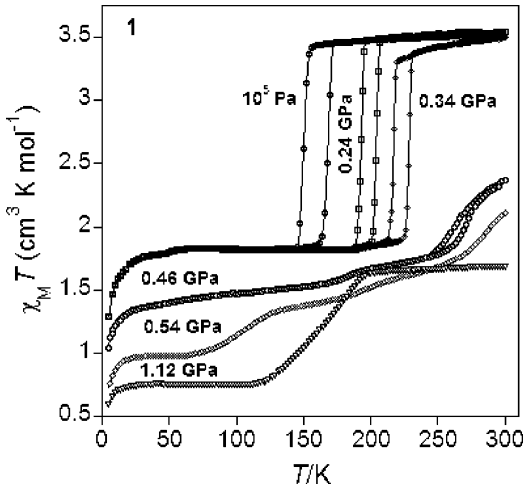

Figure 6. Temperature-dependent magnetic susceptibility measurements performed at 10^5 Pa and 0.24, 0.34, 0.46, 0.54, and 1.12 GPa for **1** (rate of measurements: 1 K min^{-1}).

state. The $\chi_M T$ product recorded in the warming mode evidences a hysteresis of 18 K width ($T_c^{\downarrow}$ = 149 K and $T_c^{\uparrow}$ = 167 K). For P = 0.24 GPa, the transition remains steep while the critical temperature for the cooling and warming modes change: $T_c^{\downarrow}$ = 192 K and $T_c^{\uparrow}$ = 203 K. A further increase of the pressure up to 0.34 GPa provokes a linear displacement of the transition to higher temperatures, while the hysteresis width remains unaltered ($T_c^{\downarrow}$ = 217 K and $T_c^{\uparrow}$ = 228 K).

In general, SCO systems follow this linear dependence of $T_c(P)$ vs P.[23,24] Furthermore, the mean-field theory of phase transitions in SCO compounds predicts a decrease of the hysteresis width and of the slope of the transition curve with increasing pressure.[23−28] The hysteresis vanishes at a critical pressure, and at even higher pressures, the transition trans-

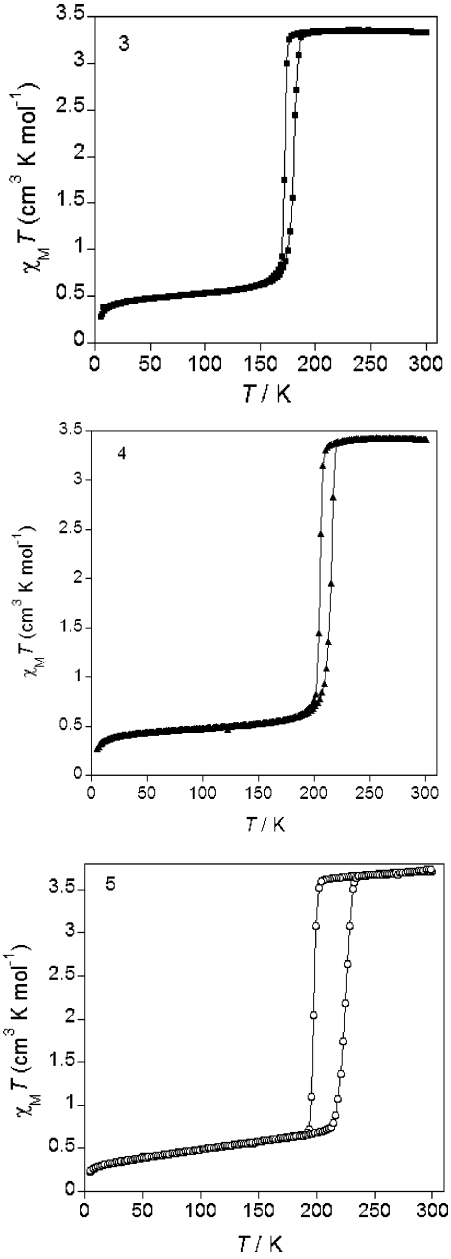

Figure 7. Temperature-dependent magnetic susceptibility measurements for **3**−**5** at atmospheric pressure (rate of measurements: 1 K min^{-1}).

forms into a second-order gradual phase transition. In fact, at pressures comprised between 0.46 and 0.54 GPa, the spin transition in compound **1** has been transformed into a second-order spin transition with more than 20% of the Fe(1) ions in the LS state (inferred from $\chi_M T$ at 300 K). Moreover, at 0.46 GPa, the onset of the spin transition in the Fe(2) ions can be appreciated at 190 K. At 0.54 GPa, practically all of the Fe(2) ions change the spin state continuously in the interval of temperatures comprised between 230 and 70 K. Finally, when pressure attains 1.12 GPa, the Fe(1) ions are in the LS configuration in the whole range of temperatures investigated (5−300 K), whereas the Fe(2) ions undergo a gradual spin transition located at $T_{1/2}$ = 162 K. Surprisingly, compound **2** does not exhibit spin-transition properties; the

(23) Gütlich, P.; Ksenofontov, V.; Gaspar, A. B. *Coord. Chem. Rev.* **2005**, *249*, 1811.
(24) Ksenofontov, V.; Gaspar, A. B.; Gütlich, P. *Top. Curr. Chem.* **2004**, *235*, 23.
(25) Usha, S.; Srinivasan, R.; Rao, C. N. R. *Chem. Phys.* **1985**, *100*, 447.
(26) Köhler, C. P.; Jakobi, R.; Meissner, E.; Wiehl, L.; Spiering, H.; Gütlich, P. *J. Phys. Chem. Solids* **1990**, *51*, 239.
(27) Romstedt, H.; Hauser, A.; Spiering, H. *J. Phys. Chem. Solids* **1998**, *59*, 265.
(28) Adler, P.; Wiehl, L.; Meissner, E.; Köhler, C. P.; Spiering, H.; Gütlich, P. *J. Phys. Chem. Solids* **1987**, *48*, 517.

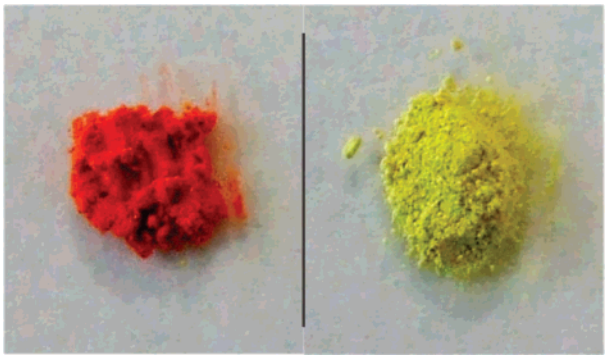

Figure 8. Change of color upon spin transition in compounds **3**−**5** (orange, LS state; yellow, HS state).

Fe^{II} centers remain in the HS state in the temperature range investigated, 5−300 K (Figure SM3, Supporting Information).

Like in **1**, the magnetic susceptibility for **3**−**5** was determined over the 5−350 K range in a field of 1 T. The $\chi_M T$ vs T plots are shown in Figure 7. In the high-temperature region, the $\chi_M T$ values are in the range 3.3−3.7 cm^3 K mol^{-1} for **3**−**5**. These values are consistent with a $S = 2$ HS ground state for an Fe^{II} ion. Upon cooling, $\chi_M T$ remains almost constant down to a temperature value from which it undergoes a sharp decrease characteristic of a first-order spin transition. For compounds **3**−**5**, the conversion to the LS state is complete, and it can also be inferred from the $\chi_M T$ values at low temperature [$\chi_M T$(5 K) = 0.39 (**3**), 0.41 (**4**), and 0.31 (**5**) cm^3 K mol^{-1}]. The warming mode reveals the occurrence of thermal hysteresis. The critical temperatures for the cooling ($T_c^{\downarrow}$) and warming ($T_c^{\uparrow}$) modes are 170 and 180 K (**3**), 204 and 214 K (**4**), and 197 and 223 K (**5**), respectively. It is worth mentioning the color change from yellow to orange observed in **3**−**5** upon spin transition (Figure 8).

Differential Scanning Calorimetry (DSC). DSC measurements for **1** and **3**−**5** were carried out in the 150−300 K temperature range at a rate of 5 K min^{-1}. The thermal dependence of the anomalous heat capacity, ΔC_p, obtained from DSC measurements is shown in Figure 9. For compound **1**, an anomaly in the heat capacity appears in the cooling mode at $T_c^{\downarrow}$ = 149 K and at $T_c^{\uparrow}$ = 168 K in the warming one, indicating the occurrence of a hysteresis 19 K wide. These values agree reasonably well with those observed from the $\chi_M T$ vs T plot. Compounds **3**−**5** exhibit anomalies in the heat capacity at $T_c^{\downarrow}$ = 172 K and $T_c^{\uparrow}$ = 180 K (**3**), $T_c^{\downarrow}$ = 204 K and $T_c^{\uparrow}$ = 214 K (**4**), and $T_c^{\downarrow}$ = 198 K and $T_c^{\uparrow}$ = 225 K (**5**), respectively, which are comparable with those obtained from magnetic data. The small differences in critical temperatures between DSC and magnetic data have their origin in the different rates at which the experiments were done. Table 3 summarizes the derived thermodynamic parameters ΔH_{SCO} and ΔS_{SCO} for compounds **1** and **3**−**5**; the values obtained are in the ranges of the values expected for cooperative spin transitions in Fe^{II} compounds.[4−6,29]

(29) Sorai, M.; Nakano, M.; Miyazaki, Y. *Chem. Rev.* **2006**, *106*, 976.

Discussion

Observation of cooperativity associated with the SCO phenomenon in monomeric Fe^{II} complexes and its rationalization in terms of effective intermolecular interactions lead to the realization that enhancement of cooperativity could be achieved by the use of bifunctional ligands, leading to polymeric compounds. Indeed, efficient propagation of the molecular changes stemming from the SCO metal ion through the crystal lattice would be improved by the covalent bonds linking the SCO centers. In this regard, utilization of metallocyanate complexes as building blocks in combination with pyridine, pyrazine, pyrimidine, or related ligands has revealed itself to be a fruitful synthetic strategy to obtain new 2D and 3D Fe^{II} SCO polymers displaying a rich variety of topologies and properties.[12−20]

In particular, self-assembly of Fe^{II}, pmd, and [Ag^I(CN)$_2$]$^-$ building blocks has originated five singular coordination polymeric networks: {Fe(pmd)$_2$[Ag(CN)$_2$]$_2$}[15] (polymorphs A and B), {Fe(pmd)(H$_2$O)[Ag(CN)$_2$]$_2$}·H$_2$O,[13b,19] {Fe(pmd)-[Ag(CN)$_2$]$_2$},[13b] and {Fe(pmd)[Ag(CN)$_2$][Ag$_2$(CN)$_3$]}.[14] The chemical diversity found in the system Fe−pmd−[Ag(CN)$_2$] arises and concerns its synthesis. All polymers were isolated as single crystals from the slow diffusion of water solutions in H-shaped vessels, with the exception of {Fe(pmd)[Ag-(CN)$_2$]$_2$},[13b] which was obtained from dehydration of {Fe-(pmd)(H$_2$O)[Ag(CN)$_2$]$_2$}·H$_2$O.[13b] Both the temperature and diffusion rate of the starting materials in the H-shaped vessels were found to be critical for the isolation of one polymer or another. Indeed, polymorphs A and B are obtained when the temperature is kept at around 303 K, while compounds {Fe-(pmd)(H$_2$O)[Ag(CN)$_2$]$_2$}·H$_2$O and {Fe(pmd)[Ag(CN)$_2$][Ag$_2$-(CN)$_3$]} are exclusively formed when the temperature is kept close to 280 K. In contrast, self-assembly of Fe^{II}, 5-Br-pmd, and [Ag^I(CN)$_2$]$^-$ using the slow-diffusion technique at different temperatures only afforded compound **1**.

As far as the crystal structure of compound **1** is concerned, it is interesting to note that this type of uninodal 3D network was not found in the polymers with the pmd ligand. Let us briefly remember the crystal structure of these last polymers. Polymorphs A and B can be viewed as 3D coordination polymers made up of a stack of a series of layers constituted of [Ag^I(CN)$_2$]$^-$ and Fe^{II} atoms defining square {[Fe(pmd)-(Ag(CN)$_2$)}$_n$ grids. The pmd ligands, which occupy the axial positions of the coordination environment around the Fe^{II} center, interact with the Ag atoms belonging to the adjacent layers, defining the 3D architectures. The architectural isomerism represented by polymorphs A and B is associated with the conformational changes occurring in the usually rigid [Ag^I(CN)$_2$]$^-$ linker. Compound {Fe(pmd)(H$_2$O)[Ag-(CN)$_2$]$_2$}·H$_2$O has two Fe sites interconnected by the [Ag^I(CN)$_2$]$^-$ linkers occupying the equatorial positions. While one Fe^{II} site has two pmd ligands in the axial positions, the other one has two molecules of water. Both sites alternate defining a highly porous net with CdSO$_4$ topology. In fact, three nets interpenetrate each other. In this polymer, the pmd ligands do not coordinate the [Ag^I(CN)$_2$]$^-$ linkers; if not, they interact via hydrogen bonding with the coordinated

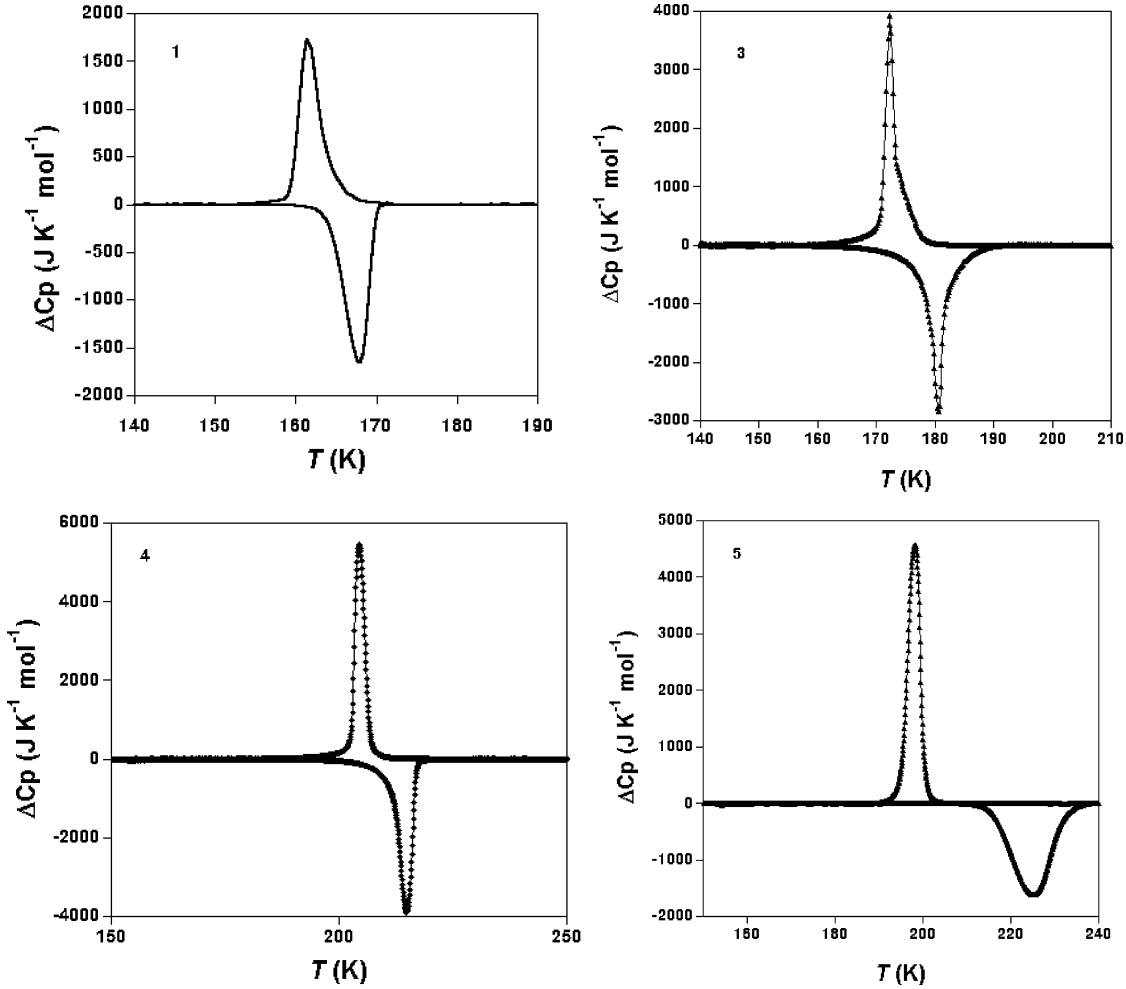

Figure 9. DSC measurements performed at a rate of 5 K min^{-1} for **1** and **3**−**5**.

Table 3. Thermodynamic Parameters ΔH and ΔS for **1** and **3**−**5** Deduced from DSC Analysis

compound	ΔH (J mol^{-1})	ΔS (J K^{-1} mol^{-1})
1	6	38
3	11	62
4	16	76
5	16	81

water molecules of the adjacent nets. Dehydration of this compound provokes a spontaneous coalescence of the three independent nets into a new 3D net, $\{Fe(pmd)[Ag(CN)_2]_2\}$, where the pmd ligands act as bridges between the Fe^{II} atoms. Compound $\{Fe(pmd)[Ag(CN)_2][Ag_2(CN)_3]\}$ is rather particular in this series of compounds because it contains the linker $[Ag_2(CN)_3]^-$, which is formed in situ during the diffusion process and defines a very complicated self-interpenetrated 3D network.

In general, the structural parameters, Fe−N bond distances and angles, Fe−N average bond length, Ag−C bond distances and angles, and Fe−Br-pmd−Fe and Fe−Ag(2)−Fe distances found for **1** at 293 and 150 K are similar to those observed in the above-discussed pmd-based 3D polymers. Another comparable fact is the presence of two different crystallographic Ag sites at 293 K, where one linker $[Ag(CN)_2]^-$ [C(1)−Ag(1)−C(1^i) = 180.0(4)°] is linear and the other is bent [C(2)−Ag(2)−C(2^i) = 168.8(5)°]. However, differences emerge in **1**: (i) the structural reorganization as a consequence of the spin state change is accompanied by a change of the space group (*C*2/*c* at 293 K and $P2_1/c$ at 150 K); (ii) there are no Ag···Ag interactions; those are prevented by the uninodal 3D network; (iii) there are no hydrogen bonds or short C···C or Br···Br interactions. The last two differences arise from the undulated nature of these planes imposed by the nonlinear $[Ag(2)(CN)_2]^-$ groups and the particular zigzag disposition of the 5-Br-pmd ligands with respect to the Fe node.

Compound **1** exhibits spin-transition characteristics at atmospheric pressure similar to those reported for pmd-based 3D polymers. Cooperative spin transitions in the temperature interval of 150−225 K accompanied by a drastic change of color (HS, yellow or orange; LS, red) are observed in most of the studied 3D polymers. This thermochromic effect is the result of an increase in the intensity of the metal-to-ligand charge-transfer (MLCT) band around 550 nm, associated with the electron delocalization from the t_{2g} orbitals of the Fe^{II} ion to the π^* orbitals of the ligands, which is enhanced by the HS → LS spin change. The overall enthalpy (ΔH) and entropy (ΔS) variations associated with the spin transition were found to be in the ranges 10−12 kJ mol^{-1} and 60−65 J K^{-1} mol^{-1}, respectively. As expected, the ΔS values are, in general, significantly larger than the entropy variation

resulting from the change in spin-only values {$\Delta S = R$ ln-$[(2S_{HS} + 1)/(2S_{LS} + 1)] = 13.4$ J mol^{-1} K^{-1} for $S_{HS} = 2$ and $S_{LS} = 0$}. The excess of entropy mainly corresponds to the structural reorganization that takes place concomitantly with the spin-state change. The structural reorganization accounts mainly for the Fe−N bond distances, which are on average 0.2 Å shorter in the LS state. The thermodynamic parameters found for **1** fall into the range of values expected for cooperative spin transitions and are comparable to those observed in the polymers with the pmd ligand. Under applied small hydrostatic pressures, compound **1** follows a linear dependence of T_c vs P and transforms into a second-order gradual phase transition at increasing pressures as the mean-field theory of phase transitions in SCO compounds predicts. In contrast, the occurrence of structural phase transitions and/or a change of the bulk modulus of the material under applied pressure have been proposed for the anomalous behavior observed in {Fe(pmd)(H_2O)[Ag($CN)_2]_2$}·H_2O,[19] e.g., an increase of the hysteresis width, a nonlinear behavior of T_c-(P) vs P. The magnetic behavior observed for **1** under applied pressure resembles more that of the cyanide polymers containing 3CN-py[30] or bpe ligands.[12]

Compound **2** was isolated using the same synthetic route as was followed for **1**. Despite many attempts to obtain single crystals of enough quality to perform X-ray determinations, the results were unsuccessful. The XRD profile of **2** acquired at 293 K points out a structure similar to that observed for **1**. The paramagnetic behavior of **2** can be understood in terms of a decrease of the crystal-field strength at the Fe centers. It is provoked by the more electronegative character of the Au atoms of the [Au($CN)_2$]$^-$ ligands in comparison with the Ag atoms. Indeed, the Au−C bond length is observed to be notably shorter than the Ag−C one. This fact is finally reflected as weaker donor and acceptor capabilities of the N atom of the [Au($CN)_2$]$^-$ ligand.[12−20]

Compounds **3**−**5** are not similar or isostructural with **1**. The information about the coordination mode of the 5-Br-pmd ligand in complexes **3**−**5** can be derived directly from the IR spectra measured at room temperature (Figure SM4, Supporting Information). For the noncoordinated 5-Br-pmd ligand, a band at 1550 cm^{-1} assigned to the C═N bond stretching of the ring is observed. It is shifted to the high-frequency region in the case of bidentate coordination. Indeed, the value of this band in coordination polymers lies typically 15−30 cm^{-1} higher compared to that of the free ligand, and for compounds **1** and **2**, the values are 1573 and 1574 cm^{-1}, respectively. When the ligand acts as monodentate, an additional band shifted to the lower frequency region is found. The intense peaks located in **3**−**5**, at 1570 and 1540 cm^{-1} (**3**), 1570 and 1539 cm^{-1} (**4**), and 1570 and 1540 cm^{-1} (**5**), strongly suggest that the ligand 5-Br-pmd acts as monodentate in compounds **3**−**5**. Considering the analytical data, the XRPD patterns, and the IR spectra of compounds **3**−**5**, one could propose a 2D structure similar to that reported for [Fe($py)_2$(M($CN)_4$)] (M = Ni^{II},[10] Pd^{II},[11] Pt^{II} [11]). It consists of 2D extended metal cyanide sheets constructed of the alternating linkage between square-planar M^{II} and octahedral Fe^{II} ions through cyano bridges. The Fe^{II} ion is octahedrally coordinated by four terminal N atoms of the cyano groups and two N atoms of two py ligands in a trans configuration.

As far as the magnetic properties and DSC profiles of **3**−**5** are concerned, it is worth mentioning that their cooperative spin transitions resemble very much those observed for [Fe-($py)_2$(M($CN)_4$)] (M = Ni^{II},[10] Pd^{II},[11] Pt^{II} [11]). In fact, the critical temperatures of the spin transitions are similar, which indicates that the 5-Br-pmd ligand imparts a ligand field similar to that of py.

In summary, the present family of polymeric iron(II) cyanide compounds adds new examples to the richness of the spin-transition properties of cyanide-based polymers. Possible applications of these materials can be foreseen as optical sensors by virtue of their thermochromic properties.

Experimental Section

Materials. 5-Bromopyrimidine (5-Br-pmd), K[Ag($CN)_2$], K[Au-($CN)_2$], K_2[Ni($CN)_4$], K_2[Pd($CN)_4$], K_2[Pt($CN)_4$], and Fe($BF_4)_2$·$6H_2O$ were purchased from commercial sources and used as received.

Synthesis of 1. The synthesis of **1** was performed under an Ar atmosphere using a slow-diffusion technique. One side of an H-shaped vessel contains a mixture of Fe($BF_4)_2$·$6H_2O$ (0.15 mmol, 50 mg) and 5-Br-pmd (0.30 mmol, 48 mg) in MeOH/H_2O (1:1; 2 mL). The other side contains a H_2O solution (2 mL) of K[Ag-($CN)_2$] (0.3 mmol, 60 mg). The vessel was filled with MeOH. Prismatic orange crystals of **1** suitable for single-crystal X-ray analysis were obtained after 3 weeks. Yield: 55%. FT-IR (KBr, cm^{-1}): ν(C−H_{ar}) 3103, 3056, ν(C≡N) 2160, ν(C═C,C═N) 1574, 1431, 1408, 1330, ν(C−N) 1194, 1170, 1158, 1128, ν(C−H in-plane) 1045, ν(C−H out-of-plane) 913, 701, 653, 444. Anal. Calcd for $C_8H_3Ag_2BrFeN_6$ (**1**): C, 17.97; H, 0.57; N, 15.72. Found: C, 18.23; H, 0.62; N, 14.22. EDXA (energy-dispersive X-ray microanalysis). Found: (33% Fe, 67% Ag); (56% Fe, 44% Br).

Synthesis of 2. The synthesis of **2** was performed under an Ar atmosphere. To a solution containing stoichiometric amounts of 5-Br-pmd (0.6 mmol, 96 mg) and Fe($BF_4)_2$·$6H_2O$ (0.3 mmol, 100 mg) in MeOH/H_2O (1:1) is added with constant stirring a solution of K[Au($CN)_2$] in H_2O (0.3 mmol, 86 mg). The resulting yellowish solution is evaporated under Ar flow, and after a few days, yellowish twinned needles of **2** unsuitable for single-crystal X-ray analysis were obtained. Yield: 60%. Compound **2** can also be obtained using a slow-diffusion technique as described for **1**. However, it was not possible to grow single crystals of **2** suitable for XRD studies. FT-IR (KBr, cm^{-1}): ν(C−H_{ar}) 3105, 3055, ν-(C≡N) 2163, ν(C═C,C═N) 1573, 1431, 1408, 1330, ν(C−N) 1195, 1172, 1157, 1127, ν(C−H in-plane) 1047, ν(C−H out-of-plane) 912, 743, 701, 655, 481. Anal. Calcd for $C_8H_3Au_2BrFeN_6$ (**2**): C, 13.48; H, 0.42; N, 11.79. Found: C, 13.72; H, 0.45; N, 11.49. EDXA. Found: (33% Fe, 67% Au); (47% Fe, 53% Br).

Synthesis of 3−**5.** The syntheses of **3**−**5** were carried out under an Ar atmosphere. To a solution containing stoichiometric amounts of 5-Br-pmd (0.6 mmol, 96 mg) and Fe($BF_4)_2$·$6H_2O$ (0.3 mmol, 100 mg) in MeOH/H_2O (1:1) is added with constant stirring a solution of K_2[M($CN)_4$] [0.3 mmol, 72 mg (Ni^{II}), 86 mg (Pd^{II}); 112 mg (Pt^{II})] in H_2O (10 mL). Compounds **3**−**5** precipitate as light-yellow microcrystalline powders immediately after the addition

(30) Galet, A.; Gaspar, A. B.; Agustí, G.; Muñoz, M. C.; Real, J. A. *Chem. Phys. Lett*. **2007**, *434*, 68−72.

of a few drops of the H_2O solution. The precipitates are filtered off, washed with H_2O, and dried under vacuum. Yield: 80% (**3**−**5**).

Compound 3. FT-IR (KBr, cm^{-1}): ν(C−H_{ar}) 3054, 3027, ν(C≡N) 2159, ν(C═C,C═N) 1568, 1540, 1422, 1403, 1333, ν(C−N) 1187, 1169, 1152, 1128, ν(C−H in-plane) 1083, ν(C−H out-of-plane) 1031, 905, 704, 636, 439. Anal. Calcd for $C_{12}H_6Br_2FeN_8Ni$ (**3**): C, 26.86; H, 1.13; N, 20.88. Found: C, 27.02; H, 1.17; N, 20.42. EDXA. Found: (50% Fe, 50% Ni); (32% Fe, 68% Br).

Compound 4. FT-IR (KBr, cm^{-1}): ν(C−H_{ar}) 3061, 3029, ν(C≡N) 2169, ν(C═C,C═N) 1570, 1539, 1424, 1402, 1334, ν(C−N) 1185, 1168, 1136, 1129, ν(C−H in-plane) 1032, ν(C−H out-of-plane) 905, 706, 636, 468. Anal. Calcd for $C_{12}H_6Br_2FeN_8Pd$ (**4**): C, 24.67; H, 1.04; N, 19.18. Found: C, 25.03; H, 1.07; N, 19.03. EDXA. Found: (50% Fe, 50% Pd); (36% Fe, 64% Br).

Compound 5. FT-IR (KBr, cm^{-1}): ν(C−H_{ar}) 3061, 3028, ν(C≡N) 2169, ν(C═C,C═N) 1569, 1539, 1424, 1401, 1334, ν(C−N) 1185, 1168, 1154, 1129, ν(C−H in-plane) 1032, ν(C−H out-of-plane) 906, 706, 636, 468. Anal. Calcd for $C_{12}H_6Br_2FeN_8Pt$ (**5**): C, 21.42; H, 0.90; N, 16.65. Found: C, 21.85; H, 0.89; N, 16.35. EDXA. Found: (48% Fe, 52% Pt); (40% Fe, 60% Br).

X-ray Crystallographic Study. Diffraction data for **1** were collected with a Nonius Kappa CCD single-crystal diffractometer using Mo Kα radiation (λ = 0.710 73 Å). A multiscan absorption correction was found to have no significant effect on the refinement results. The structures were solved by direct methods using *SHELXS-97* and refined by full-matrix least squares on F^2 using *SHELXL-97*.[31] All non-H atoms were refined anisotropically.

X-ray Powder Diffraction (XRPD). The equipment used for XRPD characterization of compounds **2**−**5** was a Seifert XRD 3003 TT diffractometer, with Bragg−Brentano geometry and a Cu tube working at 40 kV with a Ni filter (0.3 mm primary slit, 0.3 mm secondary slit, 0.2 mm detector slit, and scintillation detector).

IR Spectroscopy. IR spectra were recorded at 293 K using a Nicolet 5700 FT-IR spectrometer with the samples prepared as KBr disks.

DSC. Calorimetric measurements have been performed on samples **1** and **3**−**5** at a rate of 5 K min^{-1} using a differential scanning calorimeter (Mettler Toledo DSC 821e). Low temperatures were obtained with an Al block, which was attached to the sample holder, refrigerated with a flow of liquid N_2, and stabilized at a temperature of 110 K. The sample holder was kept in a drybox under a flow of dry N_2 gas to avoid water condensation. The measurements were carried out using around 20 mg of a powdered sample sealed in Al pans with a mechanical crimp. Temperature and heat-flow calibrations were made with standard samples of In by using its melting (429.6 K, 28.45 J g^{-1}) transition. Overall accuracies of 0.2 K in the temperature and 2% in the heat flow are estimated.

Magnetic Susceptibility Measurements under Hydrostatic Pressure. The variable-temperature magnetic susceptibility measurements were performed on small single crystals by using a Quantum Design MPMS2 SQUID susceptometer equipped with a 5.5 T magnet and operating at 1 T and 1.8−375 K. The hydrostatic pressure cell made of hardened beryllium bronze with silicon oil as the pressure-transmitting medium operates in the pressure range 10^5 Pa < P < 1.2 GPa (accuracy ≈ ±0.025 GPa). A cylindrically shaped powder sample holder with dimensions of 1 mm in diameter and 5−7 mm in length was used. The pressure was measured using the pressure dependence of the superconducting transition temperature of a built-in pressure sensor made of high-purity Sn.[32] Experimental data were corrected for diamagnetism using Pascal's constants.[33]

Acknowledgment. Financial support is acknowledged from the Spanish Ministerio de Educación y Ciencia (MEC; Grant CTQ 2004-03456/BQU), from the Generalitat Valenciana (Grant ACOMP07/110), and from the European Network of Excellence MAGMANET (Contract NMP3-CT-2005-515767-2). A.B.G. thanks the Spanish MEC for a research contract (Programa Ramón y Cajal). We also acknowledge Dr. I. Boldog for the topological classification of compound **1** performed with program OLEX2.53.

Supporting Information Available: XRPD patterns of compounds **1**−**5** at 293 K, magnetic properties of compound **2**, and IR spectra recorded at 293 K for (a) ligand 5-Br-pmd and (b−f) the compounds **1**−**5**. This material is available free of charge via the Internet at http://pubs.acs.org.

IC700993S

(31) Sheldrick, G. M. *SHELX97, Program for Crystal Structure Determination*; University of Gottingen: Gottingen, Germany, 1997.

(32) Baran, M.; Dyakonov, V. P.; Gladczuk, L.; Levchenko, G. G.; Piechota, S.; Szymczak, G. *Physica C* **1995**, *241*, 383.

(33) Kahn, O. *Molecular Magnetism*; VCH: New York, 1993.